International Micro Air Vehicle Conference and Flight Competition (IMAV2013)
17-20 September 2013, Toulouse, France

# Pitch Moment Generation and Measurement in a Robotic Hummingbird

Matěj Karásek[1], Iulian Romanescu[2] and André Preumont[1]

[1] Université Libre de Bruxelles, Brussels, Belgium
matej.karasek@ulb.ac.be, andre.preumont@ulb.ac.be
[2] "Gheorghe Asachi"Technical University Iaşi, Iaşi, Romania
iulian_romanescu@yahoo.com

**Abstract**

Micro Air Vehicles (MAVs) with flapping wings try to mimic their biological counterparts, insects and hummingbirds, as they can combine high agility manoeuvres with precision hovering flight. Near-hovering flapping flight is naturally unstable and needs to be stabilized actively. We present a novel mechanism for pitch moment generation in a robotic hummingbird that uses wing twist modulation via flexible wing root bars. A custom build force balance, sensitive enough to measure the cycle averaged pitch moment as well as lift force, is also presented. The introduced prototype mechanism generates pitch moment of up to ± 50g.mm. Finally we integrate a Shape Memory Alloy (SMA) wire to actuate the wing root bar ends. We present achievable displacement versus bandwidth as well as generated pitch moment.

## 1 Introduction

Micro Air Vehicles (MAVs) or drones start to be part of our daily lives. Apart from obvious military applications they are being utilized more and more by police, fire brigades, film-makers as well as enthusiasts because they represent a relatively inexpensive yet powerful tool for aerial photo- and videography. The most widespread MAV design of today is a propeller-equipped quadrotor or multirotor, popular for its great stability and good manoeuvrability. Nevertheless, researchers keep exploring other possible ways of propulsion such as flapping wings inspired by insects and hummingbirds, the masters in combining precision hovering with breathtaking aerial acrobacy.

Many studies have shown that the near-hover flapping flight of diptera (flies with 1 pair of wings) is naturally unstable, e.g. [11, 4]. The animal brain needs to constantly process the sensory system signals and respond accordingly to maintain the desired body attitude. In other words, it needs to generate moments around the three body axis - roll, pitch and yaw.

This can be achieved through wing motion modifications that affect the lift and drag distribution over one flapping cycle [2]. Any asymmetry in the force distribution will cause non-zero cycle-averaged moments. If for example more lift is produced in front of the body than behind the body the average pitch moment over one wingbeat will be in nose-up direction. Roll moment can be achieved simply by a difference in left and right wing average lift production. Finally, an asymmetry between average drag forces of the left and right wing will result into yaw moment. Implementing similar mechanisms into flapping-wing robots, while keeping them relatively simple and, as a result, lightweight, is what makes their development challenging.

The first tail-less flapping wing MAV to demonstrate hovering flight was developed in 2012 by AeroVironment [5] (Figure 1a). It is controlled by a mechanism called wing twist modulation that modifies the wing camber. Recently three other flyers capable of hovering have been introduced. The

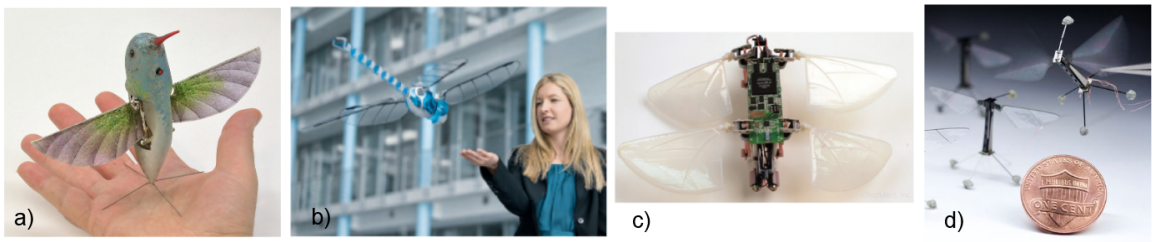


Figure 1: Existing flapping-wing robots capable of hovering: a) Nano Hummingbird (16.5 cm, 19 g), b) BionicOpter (63 cm, 175 g), c) TechJect Dragonfly (15 cm, 25 g), d) RoboFly (3 cm, 80 mg)

first two, BionicOpter by Festo [1] (Figure 1b) and Techject Dragonfly [7] (Figure 1c), use a four wing concept mimicking the dragonfly morphology. They are controlled by independent amplitude modulation of the 4 wings, moreover BionicOpter can also change their flapping plane orientation.

The last MAV is the piezoelectric-driven RoboFly from Harvard university (Figure 1d) that demonstrated the guided take-off already in 2008 [12]. The newest version [6] can be stabilized in air by controlling the amplitude and mean position of each wing independently, although the attitude sensing as well as power is still off-board.

In this work we present a novel mechanism for moment generation. It is using the wing twist modulation, similar to [5], however the mechanism is much simpler. We demonstrate that the prototype can generate lift force of 8.5g together with pitch moments of up to $\pm$ 50g.mm. Further, we explore the the possible use of Shape Memory Alloys (SMA) in control mechanism actuation.

Measurement of such small efforts in a highly vibratory system, which the flapping-wing robot certainly is, poses yet another challenge. To our knowledge none of the commercially available sensors combines sufficient sensitivity to both forces and moments with high natural frequencies preventing it from vibrating. For this reason we have also developed a 2DOF force-moment balance that is sensitive and yet stiff enough to evaluate the cycle averaged lift and pitch moment.

## 2 Robotic hummingbird prototype

The goal of our project is to develop a hummingbird sized robot with a wingspan of around 15 cm. The flapping motion is realized by a linkage mechanism that consists of two stages: a slider crank based mechanism, that generates a low amplitude rocker motion, and a four-bar linkage that amplifies the motion (Figure 2). The mechanism dimensions were optimized for the desired amplitude as well as for symmetry of upstroke and downstroke velocity profile. The gearbox has a reduction ratio of 19.75:1. The frame and the links are build by an Objet 3D printer (Eden series); the material used is DurusWhite. Aluminium and steel rivets are used to connect the links together. The mechanism is driven by a 7mm brushed DC motor.

The wings (Figure 3) are hand-build from a 15 micron thick polyester film; Carbon-fibre-reinforced polymer (CFRP) bars/bands are used as stiffeners. Their length is 70 mm and chord 25 mm. Sleeves at the leading edge and at the root edge (close to the body) are reinforced with Icarex to increase their durability. The sleeves allow easy assembly and disassembly as well as free rotation around the leading edge and root edge CFRP bars. Since the angle between the sleeves is greater than the angle between the leading edge and wing root bar the wing becomes cambered after assembly. The camber is, similarly to the Nano Hummingbird, twisted and bistable - it can passively flip from one side to

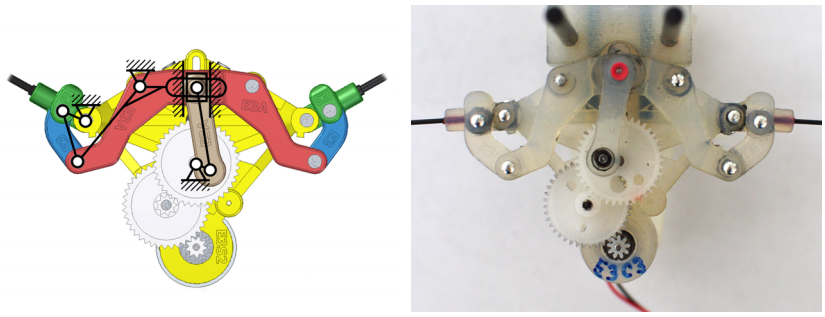

Figure 2: Flapping mechanism: model (left) and assembled prototype (right)

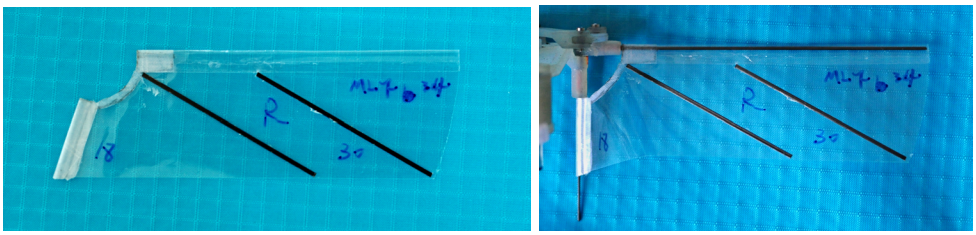

Figure 3: Polyester film wing becomes cambered after assembly.

another depending on the direction of motion.

Our best prototype so far can generate 12 g of lift while flapping at 25 Hz at a nominal voltage of 1 cell Li-Po battery (3.7 V). The robot weight, with a motor but without a battery, is approximately 8.5 g. A guided take-off with off board power has been successfully demonstrated (Figure 4).

## 2.1 Moment generation via wing twist modulation

The selected wing design allows to modify the wing twist and as a result the lift production by changing the angle between the leading edge and the root edge bar. This concept is used in the Nano

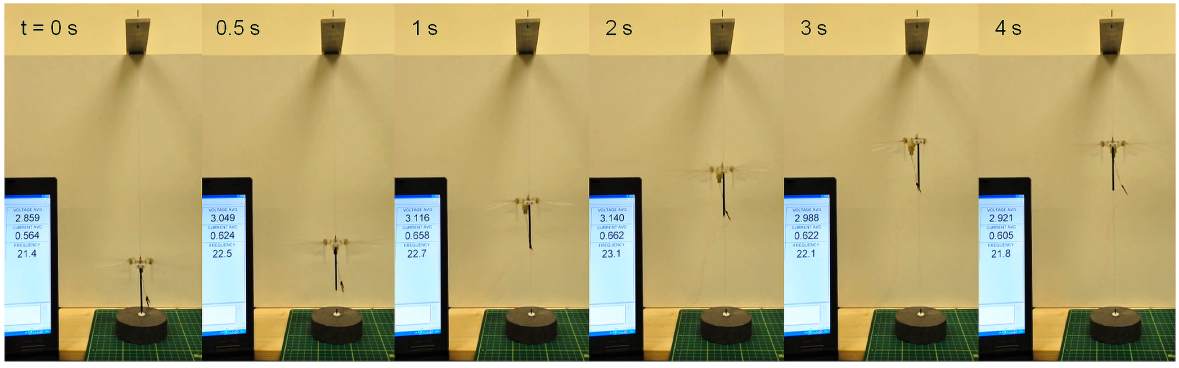


Figure 4: Take off demonstration with a guide-wire and off-board power

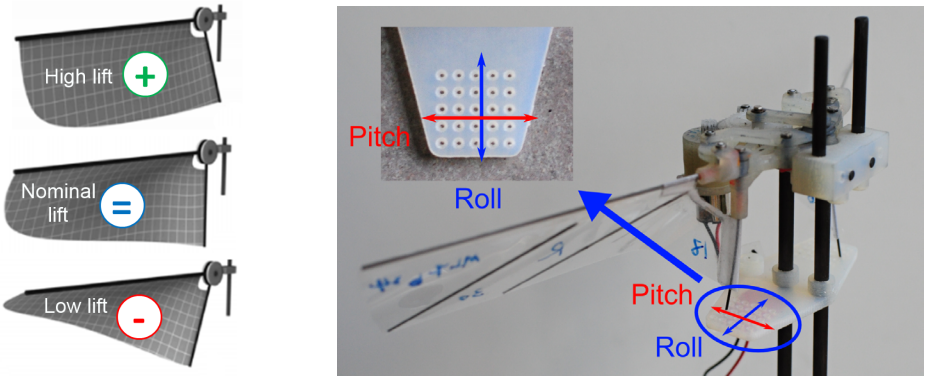


Figure 5: Wing twist modulation principle adapted from [5] (left), prototype for moment generation testing (right)

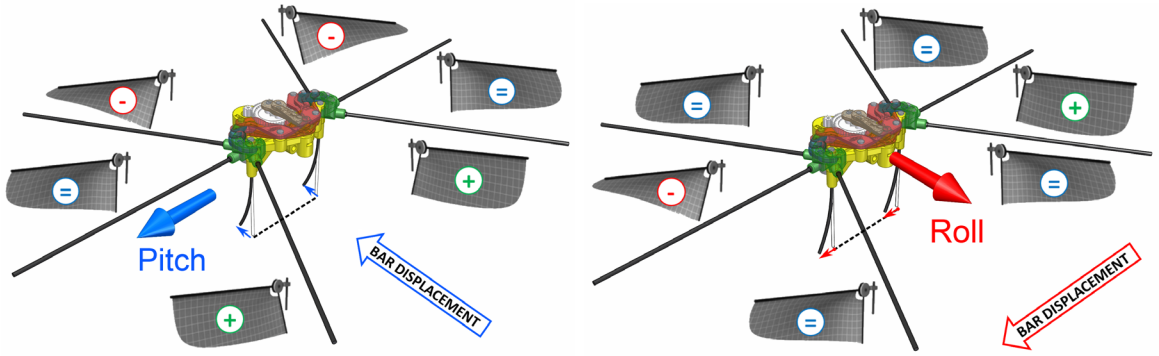


Figure 6: Moment generation via wing twist modulation: pitch moment due to front-back lift asymmetry (left), roll moment due to left-right lift asymmetry (right)

Hummingbird and is called the Variable Wing Twist Modulation [5]. For a wing with specifically optimized geometry, the lift force can be increased by moving the root bar away from the wing membrane and decreased by moving it towards the membrane (Figure 5 left).

To test this concept we have build a testing prototype (Figure 5 right). The CFRP root bars are clamped in the body frame but are flexible and their ends can be manually placed into a grid of equally spaced holes in the bottom part. The flexible bars simplify substantially the design as no joints are necessary.

The system works as follows: backward longitudinal displacement of the root bar end causes a twist (and lift) reduction when the wing is in front of the body but twist (and lift) increase when behind the body. If both left and right wing root bars are displaced in the same sense this results into a nose up pitch moment (Figure 6 left). If the root bars are displaced in the opposite sense a yaw moment is generated.

Lateral displacement of the root bars is used to generate roll moment (Figure 6 right). A deformation of one of the bars towards the body causes a decreased wing twist and thus lift reduction compared to the other wing.

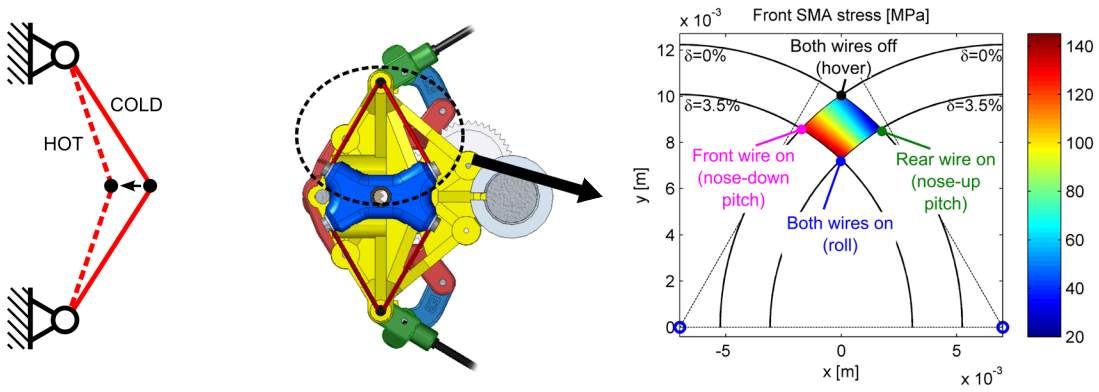


Figure 7: SMA driven control mechanism: kinematics for larger stroke (left), bottom view of the mechanism model (middle) with corresponding stress distribution for the front wire (right). The two supports are on top of each other in the bottom view.

## 2.2 SMA actuated control mechanism

The above solution is used to demonstrate and test the moment generation mechanism. In parallel we develop a control mechanism that can actively displace the bar ends to produce desired moments. The concept we present here is using Shape Memory Alloys (SMA) wires as actuators. The material uses a shape memory effect: when heated above certain temperature the crystal structure changes and, if the material is under stress, we observe contraction of the wire. After cooling the original shape is restored.

Advantages and disadvantages of using the SMA actuators in MAVs are discussed in [3]. We chose this actuator because it is very lightweight and provides directly a displacement. It can be heated simply by Joule effect. But it also has some limitations that need to be considered in the design: the maximal stroke is only about 5% of the wire length. The necessary (passive) cooling reduces significantly the bandwidth. Moreover, the material has a hysteretic behaviour due to phase transformation: the heating follows different characteristics than cooling. It can also suffer from fatigue, so operation at smaller strains (under 3.5%) and limited stresses (under 160MPa) is recommended [9].

The use of flexible bars instead of joints not only reduces the complexity, but the bar deformation also creates stress necessary for proper function of the SMAs. The small stroke achievable with a SMA wire can be overcome by the kinematics. We attach the SMA wire between two supports; the distance between these is just slightly shorter than the length of the SMA wire itself. Thus, a small contraction of the wire results in a relatively big displacement in the normal direction (Figure 7 left). The downside of this approach is that the maximal force is also reduced.

The designed system uses one pair of SMAs per wing that can displace the bar end in both longitudinal and lateral direction (Figure 7 middle). If only one of the wires is heated the bar moves diagonally in forward or backward direction, heating the two wires at the same time moves the bar laterally closer the body.

Heating the rear wires on both wings results into backward displacement of the bar ends and thus into a nose-up moment (as in Figure 6 left). Similarly heating the front wires on both wings results into a nose-down moment. Heating both wires on one wing while keeping them relaxed on the other wing results into a roll moment (similar to Figure 6 right).

The dimensions were selected to maximize the workspace while keeping the SMA wire stress under

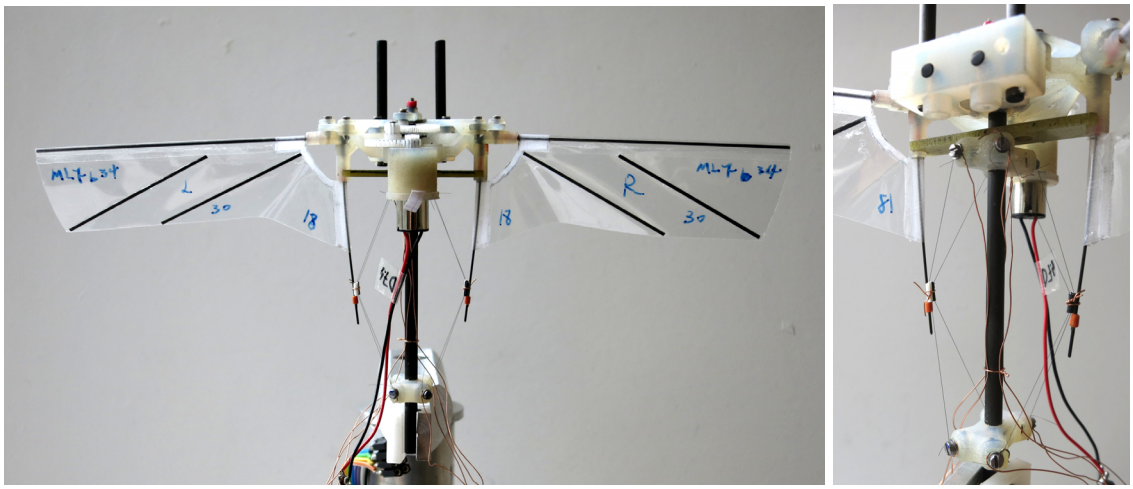

Figure 8: Robot prototype with SMA actuated control mechanism

the maximal recommended value yet high enough to assure proper phase transformation (Figure 7 right).

An important aspect that determines the mechanism bandwidth is the cycle time. While the heating phase can be accelerated by increasing the current, the cooling phase usually takes longer because the heat needs to be dissipated into the environment. The cooling is faster for wires with smaller diameter as the surface to volume ratio is higher. However, thinner wires mean also smaller maximal forces. The thinnest wire to withstand the estimated stress levels has a diameter of 50 microns.

The complete robot with the control mechanism is in Figure 8. The used SMA wires are SmartFlex®50$\mu$m [9]. Their active section is 53 mm long, the distance between the supports is 47 mm. The system to attach the SMA wires consists of two washers under the head of a bolt. The SMA wire goes around the bolt and is pressed between the washers. The power is brought by another cable, pressed by the second washer to the support.

# 3 Force balance

Measuring the efforts of a flapping wing robot is a challenging task. The generated forces are relatively small (order of 0.01 N) which requires high sensitivity. On top of that these efforts are of a periodic nature where not only the flapping frequency but also the higher harmonics are present. Hence the sensor should have a high resonance frequency.

The most frequently used commercial 6DOF force-torque sensor in the flapping wing research is the Nano-17 [10]. It is compact, it has a good sensitivity to forces (resolution of 1/1280 N $\approx$ 0.08 g ) and high resonance frequency in all DOFs (7.2 kHz). However its sensitivity to moments (resolution of 1/256 Nm $\approx$ 390 g.mm) is much lower than what we need.

Since we did not find any other suitable commercial sensor we decided to design our own force balance. To keep the design simple we only want to measure the efforts in one plane (Fx, Fz, My). Moreover, we are primarily interested in the cycle averaged efforts.

In the past we already used a precision pocket scale to evaluate the mean lift with acceptable

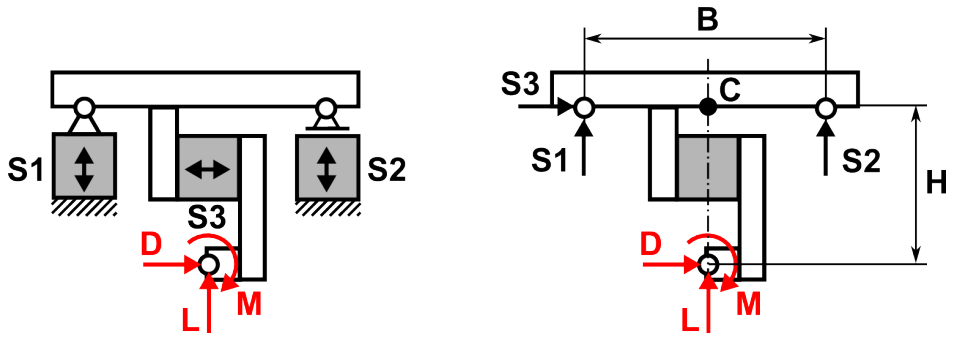


Figure 9: Schematics of the sensor (left) and its free body diagram (right)

results. The sensors used in the scales are usually double beam cantilevers with strain gages in full bridge configuration. Their advantage is that they are insensitive to the axial force as well as to the bending moment.

The experimentally determined resonance frequency of a sensor extracted from one of the scales was 210Hz, roughly 8 times the flapping frequency of our robot prototype. That is not enough to measure the time histories within one flapping cycle, but sufficient to evaluate the cycle averaged values. Thus we have selected these sensors as inexpensive yet reasonably precise base components for the designed force balance.

The balance uses three of these 1 axis force sensors in a configuration that is in Figure 9. Applying lift $L$, drag $D$ and moment $M$ on the balance results in the following sensor forces

$$\begin{aligned} S_1 &= (DH - M)/B - L/2 \\ S_2 &= (M - DH)/B - L/2 \\ S_3 &= D \end{aligned} \tag{1}$$

Sensor 3 measures directly the drag force, the sensitivity of sensors 1 and 2 to moment can be tuned by the selection of distance $B$ and $H$. From the above equations we can express the measured efforts as

$$\begin{aligned} L &= -S_1 - S_2 \\ D &= S_3 \\ M &= S_3 H + (S_2 - S_1)B/2 \end{aligned} \tag{2}$$

During the preliminary tests we have noticed that the cycle averaged drag force was very low and its effect on the moment was negligible. Thus the third sensor has been dismounted for the measurements presented here. This allows to mount the robot closer to the rotation joints and increases the resonant frequency of the system. We measure the moment with respect to the centre between the two rotation joints, $M_C$, and the equation can be rewritten as

$$M_C = (S_2 - S_1)B/2 \tag{3}$$

The distance between the two sensor joints $B$ was set to 50 mm, giving a good sensitivity yet enough space in between to fix the robot prototype. For small distance $H$ and small cycle averaged drag force $D$ the moment $M_C$ is a good approximation of the true moment $M$, with an error that can be expressed from equation (2). This has no effect on the lift force.

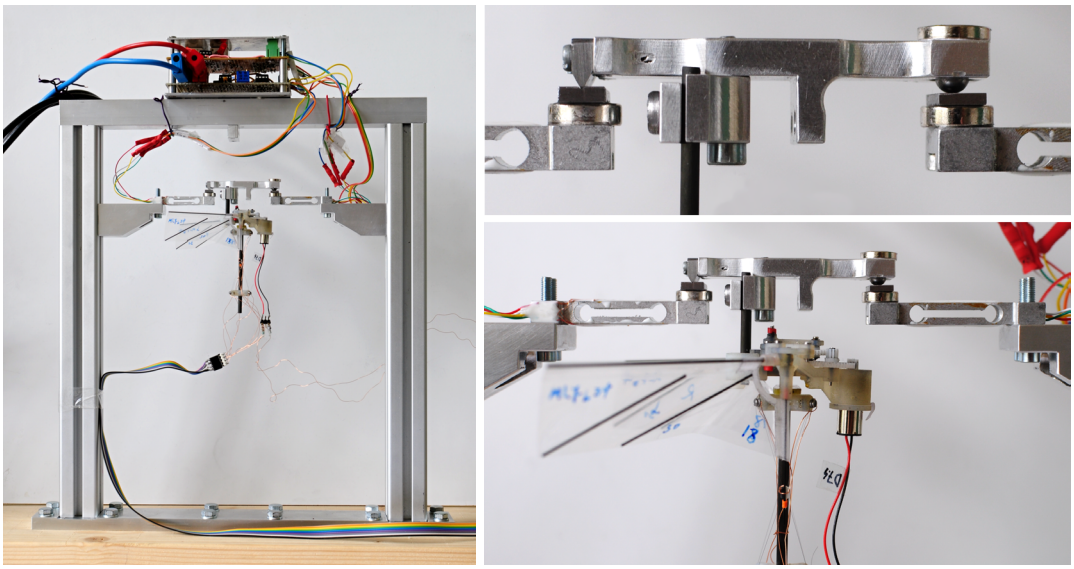

Figure 10: Force balance overview and detail views on sensors and magnetic joints

The assembled force balance is in Figure 10. Each sensor is connected to a custom build electronic circuit that provides stabilized power to the bridge and amplifies the bridge output. The sensors have been calibrated one at a time.

The rotational joints in the system should have as little friction as possible. The joint on the left is constructed as a blade inside a groove. The joint is held together by a magnetic force created by NdFeB cylindrical magnet that attracts the blade inside the groove. Both the blade and the groove are from soft magnetic steel. The joint on the right is build in a similar manner. Since it should also allow displacement to the sides, the blade was replaced by a steel ball that is touching a flat steel plate. Since the contact of the spherical ball and flat plate is only in one point, another magnet was attached on the top to increase the attracting force.

# 4 Experimental results

## 4.1 Force balance measurements

We process the force balance signals with a dSpace 1103 digital signal processor, together with the voltage and current readings of the DC motor. The flapping frequency can be detected from the motor current, because the motor torque is constantly changing due to the periodic aerodynamic and inertial forces.

The lift and moment are calculated using formulas (2) and (3). The system was designed only to measure the cycle averaged efforts due to its relatively low resonant frequency. The averaging is done online and is always calculated over a finite number of cycles. The averaging interval can be adjusted and was set to 5 seconds for the measurements presented here. The other readings (voltage, current, frequency) are averaged in the same way.

A typical lift measurement curve for a robot without control mechanism is in Figure 11. We performed the measurement 3 times in a row, each time we set the motor voltage to approximately

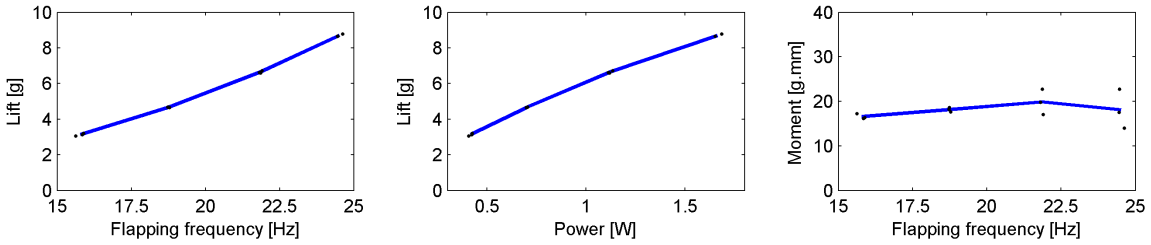


Figure 11: Force balance measurements: lift, necessary power and moment (measured values displayed as dots, lines are connecting average values).

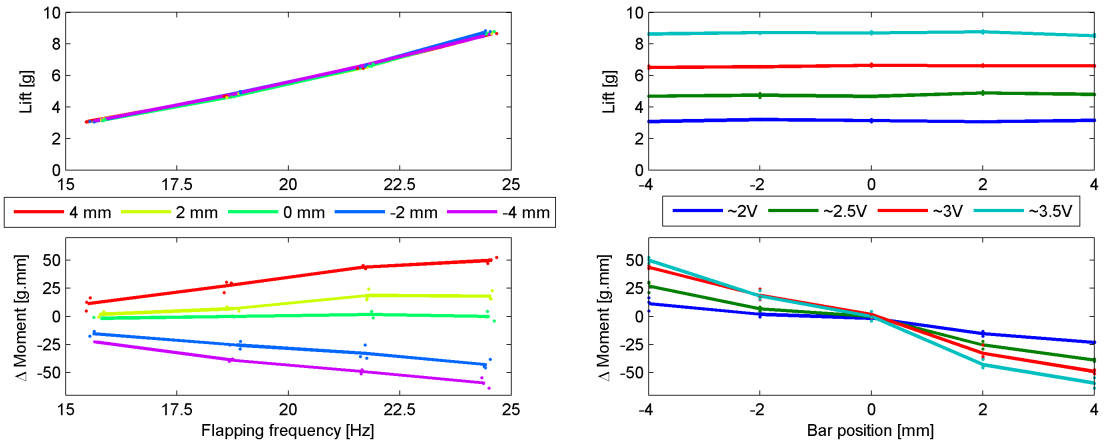


Figure 12: Lift and moment measurement results - passive bar displacement

2, 2.5, 3 and 3.5 V. The measured values are plotted as black dots, the blue line is connecting the average values. The repeatability of the lift measurements is good, with a typical standard deviation of below 0.1 g. We observe a bigger dispersion in the moment measurements, where a typical standard deviation is 5 g.mm.

## 4.2 Pitch moment generation

The main reason for designing the force balance was to demonstrate the pitch moment generation. The tests were performed with the control testing prototype with deformable wing root bars described in section 2.1 (Figure 5). The bar ends were fixed in 5 positions at 0, ±2 and ±4 mm from the centre where the root bars are straight. The measurements were carried out at 2, 2.5, 3 and 3.5 V and repeated 3 times for each position.

The results are plotted in Figure 12. Again, the individual measurements are plotted as dots and the average values connected by solid lines. The bar deformation has a negligible effect on the average lift force. The modulation of moment is approximately linear, but we can observe slightly different trend in positive and negative direction. We believe this is mostly caused by the asymmetric wing design where the stiffeners are glued only on one of the faces. When operating at 3.5 V, displacing

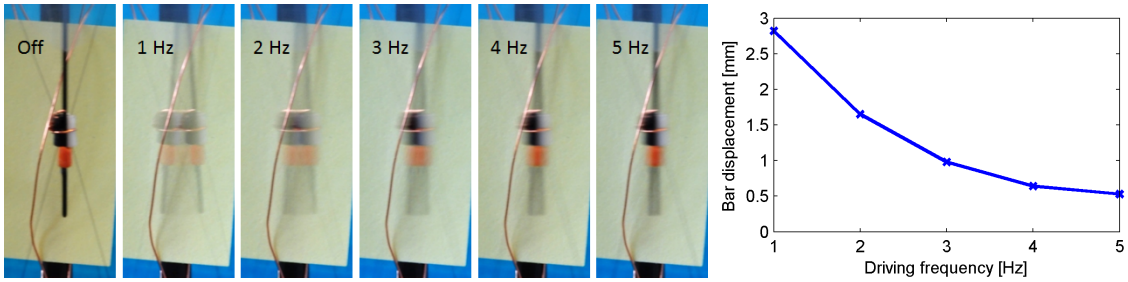


Figure 13: Long exposure images of root bar displacement by the SMA actuators driven at various frequencies (left) and processed results (right)

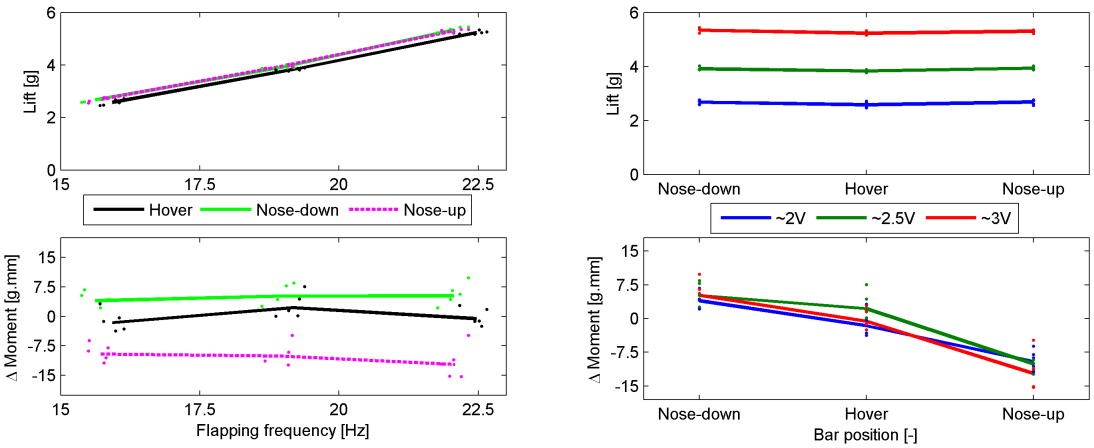


Figure 14: Lift and moment measurement results - SMA actuated bar displacement

the bars between -4 and 4 mm can generate a moment between -59 g.mm and 50 g.mm.

## 4.3 SMA driven control mechanism performance

The last tests were performed with the SMA actuated control mechanism. To determine the mechanism bandwidth we were periodically heating and cooling the front and rear pair of wires in an alternating manner, i.e. we were switching between the positions for nose-down and nose-up pitch moment. The achieved displacement was measured from a long exposure camera image. The duty cycle was 50% and the frequency was beeing changed from 1Hz to 5Hz. The current was constant during the heating phase, a value of 110mA was identified as optimal (no overheating). The airflow from the wings accelerated the cooling process.

The results presented in Figure 13 were measured at a moderate flapping frequency of about 16 Hz. The maximal displacement of 2.9 mm at 1 Hz decreases significantly as the command becomes faster. According to the results from the previous section the maximal displacement would generate a pitch moment of approximately ± 20 g.mm.

A direct pitch moment measurement was carried out in three (steady) positions according to

Figure 7 right: 1) in hover position with all the wires relaxed, 2) in nose-up moment position with the rear pair of wires heated and 3) in nose-down moment position with the front pair of wires heated. In each position the measurement was repeated five times.

The results are plotted in Figure 14; individual measurements are displayed as dots and the lines represent the average values. The lift in hover position is slightly lower when compared to both nose-up and nose-down positions. This is in accordance with our expectations, because to generate a moment the wing root bar moves also in lateral direction which stretches the wing membrane.

The maximum generated moment is approximately -11 g.mm (nose-up) and 6 g.mm (nose-down), which is much lower than ± 20 g.mm estimated from the results in previous section. We assume this might be caused by smaller bar displacements at higher frequencies due to higher stress and higher cooling rates. However, direct comparison is not completely correct as the wing design in the SMA actuated prototype had to be modified to compensate for the wing root bar deformation, that needs to be present even in hover position to create pre-stress.

The asymmetry between nose-up and nose-down moments might come from imperfections of the hand build prototype (slight misalignments of the SMA supports, small variations of the SMA wires lengths, ...).

# 5 Conclusions

We presented a new concept of pitch moment generation for a flapping wing MAV. It combines the wing twist modulation with flexible wing root bars. We demonstrated on a custom built force balance that it can generate a maximal cycle averaged pitch moment of ± 50 g.mm by displacing the bar ends by ± 4 mm.

To actively deform the wing root bars a SMA actuated control mechanism was developed. Currently it can displace the bars ends by almost ± 1.5 mm. The actuator can work at frequencies of up to 5Hz, however the displacement is significantly reduced. Direct measurements for static displacements show that pitch moments between -11 and 6 g.mm can be generated.

We have identified several weak points of the control mechanism that should be improved. Most importantly, the bandwidth as well as the achievable stroke (and thus moments) of the current system need to be increased, possibly by forced cooling and different kinematics respectively.

The attachment system of the SMA wires should be redesigned to simplify the adjustment process during the assembly and to improve the SMA lifetime, as many failures occurred there due to stress concentration. Currently we can only control the wires in an on-off manner which allows us to reach the "corners" of the workspace. A feedback control of the stroke might be implemented as the resistance of the SMA wires can be related to the strain.

As an alternative to the proposed solution, an actuator with larger stroke and higher bandwidth, such as a servomotor, might be used in future.

# 6 Acknowledgements

The research of Matěj Karásek is supported by FRIA grant from F.R.S. - FNRS in Belgium (FC 89554). The authors would also like to thank to our colleague Yanghai Nan and to internship students Neda Nourshamsi and Mathieu Dumas for their help with wing manufacturing and testing, sensor design and SMA mechanism testing.

# References

[1] Festo AG & Co. KG. BionicOpter. `http://www.festo.com/net/SupportPortal/Files/248133/Festo_BionicOpter_en.pdf`, last viewed August 2013, 2013.

[2] Steven N. Fry, Rosalyn Sayaman, and Michael H. Dickinson. The aerodynamics of free-flight maneuvers in drosophila. *Science*, 300(5618):495–498, Apr. 2003.

[3] Giorgio Guglieri and Daniele Sartori. Experimental Characterization of Actuators for Micro Air Vehicles. *International Journal of Micro Air Vehicles*, 3(2):49–59, 2011.

[4] Matej Karasek and Andre Preumont. Flapping flight stability in hover: A comparison of various aerodynamic models. *International Journal of Micro Air Vehicles*, 4(3):203–226, 2012.

[5] Matthew Keennon, Karl Klingebiel, Henry Won, and Alexander Andriukov. Development of the nano hummingbird: A tailless flapping wing micro air vehicle. *AIAA paper 2012-0588*, pages 1–24, 2012.

[6] Kevin Y. Ma, Pakpong Chirarattananon, Sawyer B. Fuller, and Robert J. Wood. Controlled flight of a biologically inspired, insect-scale robot. *Science*, 340:603–607, 2013.

[7] Jayant Ratti, Emanuel Jones, and George Vachtsevanos. The hovering and gliding multi-wing flapping micro aerial vehicle. International patent application PCT/US2012/02571, Aug. 2012.

[8] Graham K. Taylor, Robert L. Nudds, and Adrian L. R. Thomas. Flying and swimming animals cruise at a Strouhal number tuned for high power efficiency. *Nature*, 425:707–711, Oct. 2003.

[9] SAES Getters. SmartFlex Wire & Springs. `http://www.saesgetters.com/sites/default/files/SmartFlexWire&Springdatasheets_0.pdf`, last viewed August 2013, 2009.

[10] SCHUNK GmbH & Co. KG. FT-Nano-17. `http://www.schunk.com/schunk_files/attachments/FT-Nano_017_EN.pdf`, last viewed August 2013, 2013.

[11] Mao Sun, Jikang Wang, and Yan Xiong. Dynamic flight stability of hovering insects. *Acta Mechanica Sinica*, 23(3):231–246, Jun. 2007.

[12] Robert J. Wood. The first takeoff of a biologically inspired at-scale robotic insect. *IEEE Transactions on Robotics*, 24(2):341–347, Apr. 2008.